Electron correlation effect in the momentum density of copper metal

Gerrit E. W. Bauer* and Jochen R. Schneider
Hahn-Meitner-Institut für Kernforschung, Glienicker Strasse 100, D 1000 Berlin 39, Federal Republic of Germany
(Received 16 July 1984)

The total Compton profile for the ⟨110⟩ direction of crystalline copper has been measured with high statistical accuracy by a γ-ray scattering experiment. Special attention was paid to the correction of multiple photon scattering in the sample and the slight spectral contamination of the incident γ radiation. The results are discussed in conjunction with earlier measurements of the Compton profile anisotropies and existing band-structure calculations. The effect of the electron correlation on the Compton profile and the momentum density is found to be significantly larger than in the homogeneous electron gas. A correlation correction functional required by the Hohenberg-Kohn-Sham density-functional theory is calculated in the local density approximation and is shown to improve the agreement between density-functional band-structure calculations and experiment. The remaining discrepancies can be characterized by a redistribution of momentum density in reciprocal space as compared to the model of noninteracting electrons. The appearance of this nonlocal correlation effect is specific for the momentum density and does not contradict the generally good agreement between one-electron theory and other experimental results for copper. Possible origins of the effect are discussed tentatively.

I. INTRODUCTION

Under ambient conditions the electronic state of most systems can be described by a ground-state wave function, which thus attracts a lot of theoretical efforts. Photon-scattering experiments can probe the ground-state space and time correlation function of the electronic charge density of the scattering target[1] and contribute sensitive tests for theoretical models. In the limit where the recoil electron from the scattering process can be considered to be free, i.e., when the energy and momentum transfer from the photon is very large, the impulse approximation applies, and the differential cross section of initially monochromatic photons provides information about the electronic momentum density $n(\vec{p})$ via the so-called Compton profile:[2]

$$J_{\vec{h}}(q)=\int n(\vec{p})\delta(q-\vec{p}\cdot\vec{h}/h)d\vec{p}\ , \tag{1}$$

where $\vec{h}$ is the difference between the wave vectors of the scattered and the incident beam. The condition of high energy and momentum transfer is especially well satisfied for the backscattering of high-energy photons, as it happens for instance in the Compton spectrometer of the Hahn-Meitner-Institut[3] (HMI), which utilizes the 412-keV radiation of neutron-activated gold and which works at a scattering angle of 165°.

Due to the impetus of the newly developed experimental technique of angular-resolved photoemission spectroscopy,[4] theories which aim at the understanding of the electronic structure of crystalline materials have been concentrated mainly on the calculation of the electronic band structure, i.e., the eigenvalues of an effective one-particle Schrödinger equation. It should be quite clear, however, that the energy spectrum is only one aspect of the electronic properties and a theory which is not able to reproduce the results of different experiments is incomplete at best. Because of the simplicity of the experimental setup, the well-understood scattering cross section and the straightforward data analysis, Compton-scattering experiments are well suited to deliver quantitatively reliable and easily interpretable data which are useful for testing theoretical models. It should be mentioned here that the accurate determination of crystal structure factors of the electronic charge density serves the same purposes.[5,6]

The present paper is the fourth in a series on the Compton profile and the momentum density of copper. Whereas in previous work[7–9] the emphasis was put on the Compton-profile anisotropies, the total experimental Compton profile is discussed here,[10] which is considerably more difficult to measure if high accuracy is desired. The opportunity is met to discuss the observed electron correlation effect from different viewpoints.

The experimental problems, which are the photon multiple scattering and to a lesser extent the slight nonmonochromaticity of the incident γ radiation, are the subject of Sec. II. In Sec. III the observations are explained in terms of an electron correlation effect which is identified to be due to a redistribution of the occupation numbers of the band states, which is quantified by a simple model. The experimental Compton profile is then compared with existing band-structure calculations[11,12] and the results are discussed in the context of the Hohenberg-Kohn-Sham density-functional formalism.[13–16] In Sec. IV we will finally discuss why the presently available theoretical models and methods do not cope with the problem revealed in the Compton profile of copper, in the hope of motivating new theoretical efforts.

II. EXPERIMENTAL

Our aim is the accurate determination of a total directional Compton profile of copper to sort out the addition-

al information it contains as compared to the previously measured Compton-profile anisotropies.[7,17] Unfortunately the total profile is affected by several experimental errors which are expected to cancel to a large extent in the Compton profile anisotropies but have to be corrected more carefully for the total profiles.

The main problem is the fact that the photons reaching the detector may have been scattered more than once in the sample.[18] The importance of the multiple scattering becomes clear by inspection of Fig. 1, where the results of the measurements on copper single crystals are displayed as a difference between experiment and theory[11] (see Sec. III B). The samples were four discs of different thicknesses (0.6, 1.0, 1.4, and 3.0 mm) and square lateral dimensions of 4×4 cm^2, which is much larger than the area illuminated by the source (~2 cm^2) and seen by the detector (~3 cm^2). The experimental data from different measurements on the same samples have been treated separately by the conventional data processing.[19] They showed good reproducibility, and were averaged to improve the statistical accuracy. For negligible multiple scattering all runs should give identical results. The large differences shown in Fig. 1 indicate the seriousness of the problem, which exists even for the thinnest 0.6-mm sample. For the 3-mm sample every fourth photon is scattered more than once (see below).

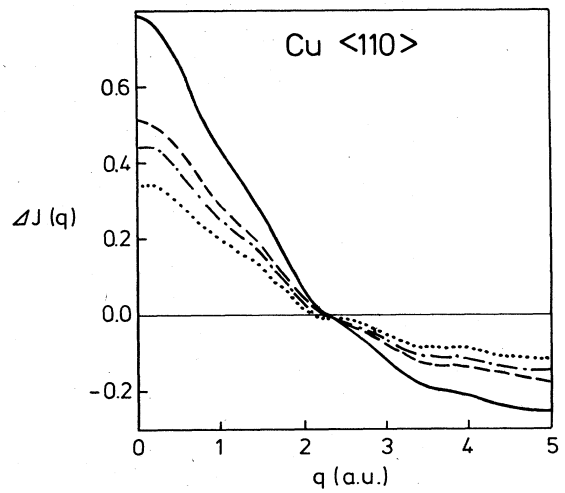

FIG. 1. Difference between the theoretical (Ref. 11) (see Table II) and the experimental Compton profiles for the ⟨110⟩ direction for samples of different thicknesses *before* the multiple scattering correction: Solid line, 3.0-mm sample; dashed line, 1.4-mm sample; dashed-dotted line, 1.0-mm sample; dotted line, 0.6-mm sample. The statistical error is hardly visible on this scale.

Another problem which becomes significant for the measurement of total Compton profiles, especially of heavier compounds, is the slight nonmonochromaticity of the primary beam, which is mainly due to inelastic scattering processes inside the γ-ray source itself. In the following both problems addressed above will be discussed in more detail and the measured profiles will be corrected for it. By this treatment we believe to have determined an experimental total profile which is more accurate than the previously published ones. The corrections are isotropic and the results for the anisotropies[7,17] remain valid, however.

A. Multiple scattering correction

The currently employed methods to correct for the effect of multiple scattering can be separated roughly into three categories. A purely empirical approach is for example an extrapolation procedure, where measurements on different sample thicknesses are extrapolated to zero thickness,[20] with the aim to obtain a Compton profile which no longer contains any multiple scattering effects. An undesirable feature of this approach is the fact that the extrapolation is certainly not linear and some linearizing function of the sample thickness has to be guessed. A well-defined approach is provided by the computer simulation of the scattering process, referred to as the Monte Carlo method.[18] Problematic are the necessary assumptions for the scattering cross section, which are difficult to verify. The third category are hybrid methods, where one tries to combine the advantages of both approaches, which are then called semiempirical. The method in Ref. 21 consists, for example, of the calculation of the ratio of the total multiple to single scattering for samples with different thicknesses for which experimental profiles must be available. The results for each profile point of measure-

TABLE I. Results of the Monte Carlo computer simulation of the multiple scattering for the Compton-scattering experiments on copper single crystals. $J^{\rm expt}(0)$: Maximum of the experimental Compton profile before correction for multiple scattering. $J^{\rm corr}(0)$: Maximum of the experimental Compton profile after correction for multiple scattering. $x_1=N_d/(N_s+N_d)$, $x_2=(N_d+N_t)/(N_s+N_d+N_t)$, $x_3=N_d^i/(N_s^i+N_d^i)$, $x_4=(N_d^i+N_t^i)/(N_s^i+N_d^i+N_t^i)$, where (N_s,N_d,N_t), respectively (N_s^i,N_d^i,N_t^i), are the number of single, double, or triple scattered photons which are detected in the total (t), respectively, interest region $(-7,7)$ in atomic units of momentum.

Sample thickness (mm)	$J^{\rm expt}(0)$ (a.u.$^{-1}$)	$J^{\rm corr}(0)$ (a.u.$^{-1}$)	x_1 (%)	x_2 (%)	x_3 (%)	x_4 (%)
0.6	4.945	5.226	10.22	11.04	8.00	8.27
1.0	4.849	5.233	13.83	15.27	10.97	11.50
1.4	4.779	5.260	16.95	19.05	13.62	14.42
3.0	4.509	5.243	25.06	29.28	20.86	22.76

ments on at least two thicknesses are then linearly interpolated to zero with respect to the multiple scattering ratio. A negative aspect is the fact that in the case of rather thick samples the extrapolation may get very inaccurate. This is indeed the case for the present measurements, as can be seen from Table I, where the results of the multiple scattering parameter from the Monte Carlo computer simulations discussed below are listed. Even for the thinnest sample the multiple scattering amounts to about 10% and one finds that the extrapolation is very sensitive to slight modifications of the experimental profiles, reflected by an increase of the statistical error which is intolerable for the present purposes.

The strategy proposed and applied here should also be understood as being semiempirical. Although the *ab initio* Monte Carlo method is used to correct individual profiles, we do not rely completely on the absolute correctness of the assumptions for the scattering cross section and the input parameter settings. The justification for the final results is based instead on the agreement of corrected profiles which have originally been affected by different amounts of multiple scattering. This approach also provides for an estimate of the systematic errors introduced by the correction procedure, which turn out to be much larger than the statistical error here. The only parameter presently available to vary the amount of multiple scattering is the sample thickness. A second independent handle on the problem of the verification of the multiple scattering correction is the availability of a tunable wavelength source, as could be provided by the hard radiation from the wiggler magnet at a synchrotron.[22] In the meantime a Compton spectrometer with a second radioactive source at a significantly different energy than the 412-keV line used here should prove to be very valuable.

The Monte Carlo computer program is described in Ref. 23 and has been made available to us by J. Felsteiner. The cross section employed takes into account elastic scattering, photoelectric absorption, and Compton scattering, where the latter is treated in the impulse approximation,[2] for which it is necessary to provide the program with an input Compton profile. It is possible to use the experimental profile to this aim, which requires an iteration to self-consistency, however. The spherical average of the copper valence-electron Compton profile for which high-quality band-structure calculations are available,[11] augmented by the core profiles from Ref. 24, has been employed instead. Up to three scattering processes have been traced for each incoming photon, since the triple scattering turned out to be rather significant (see Table I). For each run about 3 million photons have been generated, which took 4 h of CPU time on a Fujitsu FACOM IV computer. The final results are displayed in Fig. 2, again as a difference plot with respect to the band-structure calculations.[11] Note the change of scale compared to Fig. 1, which makes a periodic modulation visible, which is interpreted as the nonlocal correlation effect to be discussed in Sec. IV. The four profiles in Fig. 2 are again averaged to improve the counting statistics to better than 0.1% at the profile peak, which is more than three times smaller than the differences between the profiles in Fig. 2, which reflect the systematic error estimated to be 0.3%.

B. Nonmonochromaticity of the source radiation

The Compton source is a cylindrical piece of gold with 4-mm length and 3.5-mm diameter. After activation it has been transferred into the source holder of the HMI γ-ray diffractometer[5,6] such that the cylinder was aligned parallel to the beam direction. The energy spectrum could then be recorded directly by an intrinsic germanium solid-state detector and is plotted in Fig. 3, normalized to

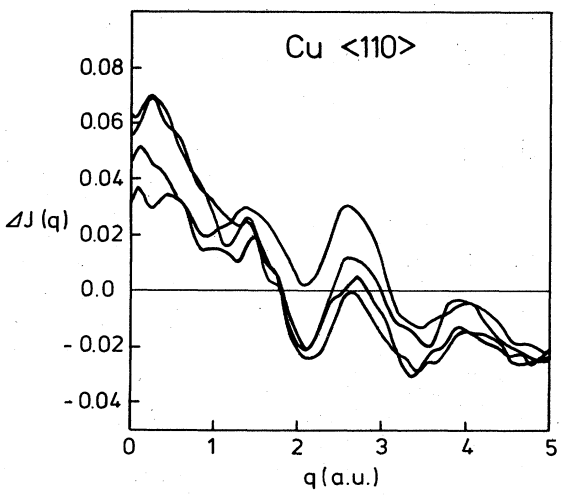

FIG. 2. Difference between the theoretical (Ref. 11) (see Table II) and the experimental Compton profiles for the ⟨110⟩ direction for samples as in Fig. 1 *after* the multiple scattering correction. The systematic error estimated from the scatter of the different profiles is clearly larger than the statistical error in the individual curves.

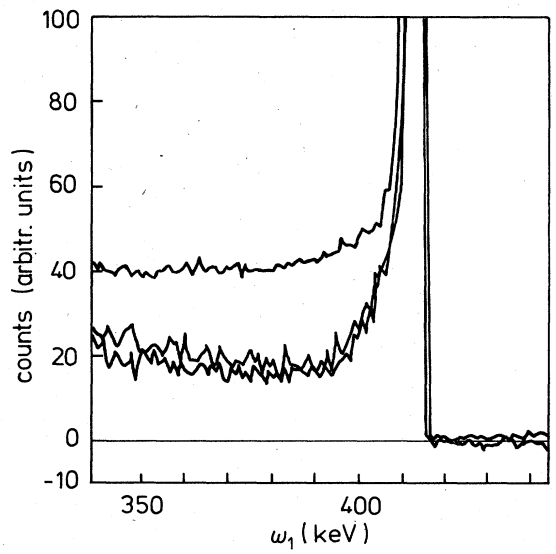

FIG. 3. Comparison of the pulse-height spectra of the direct Compton source radiation (upper curve) and those reflected at the 222 and 333 Bragg reflections of a copper single crystal. The background is subtracted, and the maximum intensity is normalized to 10^4 counts/channel.

10^4 counts at the peak. It can be seen that the main line is affected by a low-energy contamination, which is partly due to the inelastic scattering in the source itself which we want to determine, but also due to the incomplete charge collection in the detector which results in an asymmetric resolution function. The resolution function equals the measured spectrum for a point source of 412-keV radiation. Alternatively we can use the diffractometer facility to select a monochromatic beam of 412-keV γ radiation which is then used to determine the detector resolution function for this energy. The resolving power of a crystal spectrometer increases with the order of the Bragg reflection which is used. From the good agreement of the spectral distribution for the 412-keV beam reflected at 222 and 333 shown in Fig. 3, one can conclude that the remaining tail is not influenced by the source contamination anymore, but represents a genuine detector property. The deconvolution of the direct-beam measurement with the detector resolution determines the contamination, and is approximately equal to the difference between the counts in the tail region in Fig. 3. To be more precise the final experimental result for the relative intensity of the contamination as a function of energy (<412 keV) is described by the linear relationship $[0.08-0.0001(412-\omega)]\%/\text{keV}$ with an estimated error of $\pm 0.01\%/\text{keV}$. This contamination could be diminished by smaller sources which would imply a loss of intensity, however.

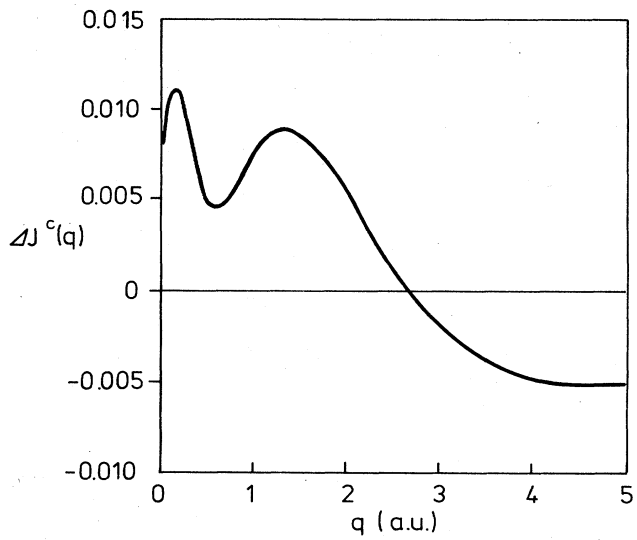

FIG. 4. Correction term for the experimental profile due to the spectral contamination of the HMI gold source for copper (see text).

The calculation of the source scattering effect by Monte Carlo computer simulation gives good agreement with the experimental result, but its description will be given elsewhere.[25]

TABLE II. $J^{\text{theor}}(q)$ is the sum of the valence-electron Compton profile of the LCAO band-structure calculation (Ref. 11) and the free atomic Hartree-Fock core Compton profile (Ref. 26) convoluted by the experimental resolution function, which is a Gaussian with full width at half maximum of 0.41 a.u. (Ref. 7). $J^{\text{expt}}(q)$ is the average of the corrected experimental Compton profiles in Fig. 2 after correction for the nonmonochromaticity of the source radiation (Fig. 4).

q (a.u.)	$J^{\text{theor}}(q)$ (a.u.$^{-1}$)	$J^{\text{expt}}(q)$ (a.u.$^{-1}$)	q (a.u.)	$J^{\text{theor}}(q)$ (a.u.$^{-1}$)	$J^{\text{expt}}(q)$ (a.u.$^{-1}$)
0.0	5.289	5.248	2.6	1.804	1.792
0.1	5.268	5.225	2.7	1.713	1.703
0.2	5.204	5.160	2.8	1.623	1.616
0.3	5.104	5.060	2.9	1.536	1.533
0.4	4.969	4.925	3.0	1.451	1.454
0.5	4.803	4.762	3.1	1.371	1.382
0.6	4.614	4.578	3.2	1.297	1.311
0.7	4.418	4.388	3.3	1.229	1.245
0.8	4.229	4.206	3.4	1.168	1.187
0.9	4.057	4.038	3.5	1.116	1.132
1.0	3.901	3.886	3.6	1.070	1.084
1.1	3.757	3.744	3.7	1.029	1.040
1.2	3.616	3.605	3.8	0.990	0.996
1.3	3.473	3.460	3.9	0.952	0.956
1.4	3.324	3.308	4.0	0.914	0.918
1.5	3.169	3.157	4.1	0.876	0.882
1.6	3.010	3.005	4.2	0.840	0.848
1.7	2.850	2.847	4.3	0.805	0.814
1.8	2.693	2.697	4.4	0.771	0.783
1.9	2.543	2.557	4.5	0.740	0.755
2.0	2.405	2.424	4.6	0.711	0.728
2.1	2.282	2.302	4.7	0.685	0.703
2.2	2.173	2.189	4.8	0.663	0.681
2.3	2.075	2.082	4.9	0.642	0.660
2.4	1.983	1.982	5.0	0.622	0.640
2.5	1.893	1.886			

In the present context the most important question is the estimation of the effect of the γ-line contamination on the measured profiles. It can be shown[26] that the cross section for the contaminated beam can be described by a convolution of the cross section of monochromatic photons by a function consisting of a δ function and a linear low-energy tail. This is equivalent to a convolution of the actual Compton profile by $[0.86+0.005q\Theta(-q)+100\delta(q)]$ a.u.$^{-1}$, where the step function $\Theta(-q)$ is zero for $q>0$ and unity elsewhere.[26]

It thus turns out that a sizable asymmetry is introduced by the nonmonochromaticity of the incident beam, which, however, is partly compensated again by the routine analysis of the raw data.[19] To find out how our final experimental profiles are affected we proceeded as follows. An atomic Compton profile of copper has been convoluted first by the experimental resolution function at the Compton energy ($\sim$160 keV), i.e., Gaussian with a full width at half maximum of 0.41 a.u. This profile is folded by the source contamination profile and subsequently fed through the conventional data processing, where the profile peak is determined by a parabola fitting routine.[19] The difference between the output and the originally symmetric profile gives the actual error in the atomic profile introduced by the spectral contamination. This difference can also be used as a correction term for experimental profiles and is plotted in Fig. 4. By comparison with Fig. 2 it becomes clear that the correction is not very significant compared to the experimental error. Its importance increases, however, with the nuclear charge of the atoms in the sample and will be larger than 1% in the profile peak for, e.g., cerium.[26] The final experimental result, including the correction term for the source contamination is listed in Table II and will be used in the following.

III. INTERPRETATION OF THE EXPERIMENTAL RESULT

As mentioned in the Introduction, we believe that the present results should be useful in the process of improving the understanding of the electronic ground state. The Compton profiles of copper as obtained by band-structure calculations can be considered to be well understood[8–12,27] and this point will be discussed here only briefly. Of special interest are the deviations of the measurements from the predictions of the one-particle model, i.e., the so-called correlation effect.

The present chapter is split into three parts. It is shown first that the observed correlation effect can be characterized by a single number. The comparison with band-structure calculations is then carried out in the second part with special emphasis on density-functional theory.[13,14] In the third part the nonlocal correlation effect[10] is described which is not explained by present theories.

A. Magnitude of the correlation effect

It is possible to reduce the information content of the experimental Compton profile to achieve a measure of the magnitude of the correlation effect without resorting to high-quality band-structure calculations at all. To this end consider the following function:[28]

$$Z(\vec{k})=\sum_{\vec{G}} n(\vec{k}+\vec{G}) , \tag{2}$$

where the sum is over all reciprocal-lattice vectors $\vec{G}$. $Z(\vec{k})$ is periodic in momentum space, so that one can restrict attention to the wave vectors $\vec{k}$ inside the first Brillouin zone. Integration of (2) over the first Brillouin zone must yield the number of particles. In the one-electron model the momentum density reads

$$n(\vec{p})=\sum_{\vec{k}\nu}^{\text{occ}} |\langle \vec{p} | \vec{k}\nu\rangle|^2 . \tag{3}$$

In Eq. (3) only those Bloch states $|\vec{k}\nu\rangle$ with crystal momentum $\vec{k}$ and band index ν contribute to the density, whose energy is smaller than the chemical potential μ, which in the case of a metal coincides with the Fermi energy. By substitution of (3) into (2) one finds

$$Z(\vec{k})=\sum_{\vec{G}}\sum_{\vec{k}'\nu}^{\text{occ}} |\langle \vec{k}+\vec{G} | \vec{k}'\nu\rangle|^2=\sum_{\vec{k}'\nu}^{\text{occ}} \delta_{\vec{k},\vec{k}'} , \tag{4}$$

where the last expression follows from the normalization condition for the Bloch states:

$$\sum_{\vec{G}} |\langle \vec{k}+\vec{G} | \vec{k}\nu\rangle|^2=1 . \tag{5}$$

In Eq. (3) the number of occupied bands ν for a specified crystal momentum $\vec{k}$ are counted. In the one-electron model $Z(\vec{k})$ is thus a constant for insulators and depends only on the shape of the Fermi surface in the case of a metal. This property becomes very useful to map a Fermi surface out of the measured angular correlation of positron annihilation radiation,[28] which in this context is usually referred to as the "Lock-Crisp-West" theorem.[29]

Equation (3) can be generalized for a many-body system in different ways. We prefer to proceed via the Green-function formalism,[30] which has the advantage that Compton scattering is incorporated into a large body of different experimental techniques, which probe one-particle excitation properties like the electronic band structure (see Sec. IV B). The momentum density is expressed as the energy integral over the diagonal elements of the spectral density function in momentum space, $A(\vec{p},\vec{p};\omega)$, which is equal to the imaginary part of the Green function $\text{Im}[G(\vec{p},\vec{p};\omega)]/\pi$ (Ref. 30):

$$\begin{aligned} n(\vec{p})&=\int_{-\infty}^{\mu} A(\vec{p},\vec{p};\omega)d\omega \\ &=(1/\pi)\int_{-\infty}^{\mu} \text{Im}[G(\vec{p},\vec{p};\omega)]d\omega . \end{aligned} \tag{6}$$

The spectral density function can be diagonalized for each energy ω by a set of energy-dependent Bloch-type orbitals $|\vec{k}\nu(\omega)\rangle$, so that

$$n(\vec{p})=\int_{-\infty}^{\mu}\sum_{\vec{k}\nu} |\langle \vec{p} | \vec{k}\nu(\omega)\rangle|^2 A_{\vec{k}\nu}(\omega) . \tag{7}$$

Substitution of (7) into (2) now yields

$$Z(\vec{k})=\sum_{\vec{k}'\nu}^{\text{occ}} Z_{\vec{k}'\nu}\delta_{\vec{k},\vec{k}'} , \tag{8}$$

where

$$Z_{\vec{k}\nu}=\int_{-\infty}^{\mu} A_{\vec{k}\nu}(\omega)d\omega \ . \tag{9}$$

We see that the energy-dependent diagonalizing orbitals do not appear anymore in $Z(\vec{k})$, so that the many-body effect is reflected only by a renormalization of the band occupation numbers from unity to a number $0\leq Z_{\vec{k}\nu}\leq 1$ (Ref. 30). In the pole approximation Eq. (8) can be understood as a sum over the residues $Z_{\vec{k}\nu}$ of the poles below the Fermi energy of the analytical continuation of $A_{\vec{k}\nu}(\omega)$ (or the Green function) in the complex energy plane.

Information about $Z(\vec{k})$ from the experimental Compton profiles is most conveniently obtained via its Fourier transform:[28,31]

$$B(\vec{r})=\int e^{iq|\vec{r}|}J_{\vec{h}}(q)dq=\int e^{i\vec{p}\cdot\vec{r}}n(\vec{p})d\vec{p} \ , \tag{10}$$

where $\vec{r}$ is parallel to $\vec{h}$. $B(\vec{R})$ is equal to the Fourier coefficients of $Z(\vec{k})$ where $\vec{R}$ is a direct lattice vector. The limited resolution of present Compton scattering experiments prevents the determination of the finer structures of the Fermi surface, i.e., the higher Fourier coefficients cannot be measured. This is reflected by the fact that the experimental profiles do not show any evidence about the Fermi surface "neck" of copper. This in contrast to the results from the positron-annihilation technique,[28] which can achieve a four-times-better resolution in momentum space than the Compton experiment reported here. It is essentially only the first Fourier coefficient $B(\vec{R})$ with $\vec{R}=(1,1,0)a/\sqrt{2}$ which can be determined reliably. This quantity turns out to be insensitive to the deviation of the actual copper Fermi surface from the free-electron sphere[7] (see Table III). Since the theoretical Fermi surfaces agree well with the measured ones, obtained for example from the de Haas–van Alphen effect, one can only conclude that an electron correlation effect must exist such that the occupation numbers $Z_{\vec{k}\nu}$ are not all unity anymore.

We define the electron correlation effect here as the deviation of the experiment from the predictions of the independent electron picture, which is

$$Z^{\text{non}}(\vec{k})=\begin{cases}12 & \text{for } \vec{k} \text{ inside the Fermi surface ,}\\ 10 & \text{for } \vec{k} \text{ outside the Fermi surface ,}\end{cases} \tag{11}$$

for the valence electrons of copper. The effect can be quantified in terms of a parameter of a simple model. Assume that the renormalization effect reduces $Z(\vec{k})$, the sum over the occupation numbers, by a constant amount $2z$ inside the Fermi surface, which corresponds to a constant increase of $2z$ outside the Fermi surface (see Fig. 5). The factor of 2 is included to take account of the spin degeneracy. For this model Eq. (5) becomes

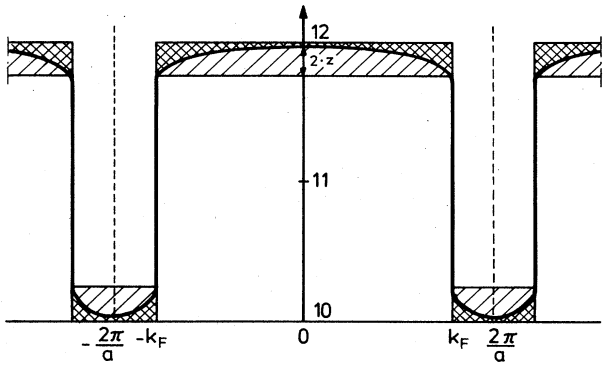

FIG. 5. Plot of $Z(\vec{k})$ of the valence electrons of copper for the X direction of the fcc Brillouin zone. The dashed area indicates the renormalization due to the electron correlation as resolved by the experiment. Also indicated are the occupation numbers for the homogeneous electron gas for $r_s=\sqrt[3]{(3/4\pi)\rho}=2$ (Ref. 32). (The average density for the $4s$ electron corresponds to $r_s=2.7$, the total density r_s does not exceed 1.9, however.)

$$B^{\text{int}}(\vec{R})=\int_{k\in\text{FS}} e^{i\vec{k}\cdot\vec{R}}(12-2z)d\vec{k}$$

$$+\int_{k\notin\text{FS}} e^{i\vec{k}\cdot\vec{R}}(10+2z)d\vec{k} \ , \tag{12}$$

$$=(1-2z)B^{\text{non}}(\vec{R}) \ , \tag{13}$$

where B^{non} is the Fourier transform of Eq. (11). z can be determined from Eq. (13) and Table III to be 0.12 ± 0.02. This result is rather surprising, since the corresponding quantity of the homogeneous electron gas, i.e., the average value of the occupation numbers within the Fermi sphere is for the valence electron density of copper only about half as large,[32] as can be seen in Fig. 5. This rather profound increase is expected to correspond to a reduction of

TABLE III. Fourier transform $B(\vec{R})$ of theoretical and experimental Compton profiles of copper for $\vec{R}=(a/\sqrt{2})(1,1,0)$. The experimental resolution is treated by a factor of $\exp[-(|\vec{R}|/8.12)^2]$.

	Free electron	Ref. 11	Ref. 12	Experiment
Without resolution	0.212	0.208	0.206	
Resolution included	0.149	0.146	0.145	0.112±0.007

the weight of the Landau quasiparticle, which must be due to a correlation of the free electrons with the 3*d* shell. This should have significant consequences for the Landau parameters which are of importance for the theory of, e.g., transport properties or the spin susceptibility.[30]

B. Density-functional theory

The only first-principles theory which to our knowledge has been applied to the calculation of the Compton profiles of transition metals is the density-functional theory of Hohenberg, Kohn, and Sham.[13,14] This formalism gives an algorithm which, in principle, allows for an exact calculation of the total energy and the charge density of the many-body system via the self-consistent solution of a set of band-structure equations ("Kohn-Sham equations"):

$$\{-\nabla^2+V_H[\rho](\vec{r})+V_{\text{ext}}(\vec{r})+V_{\text{xc}}[\rho](\vec{r})\}\phi_i(\vec{r})=\epsilon_i\phi_i(\vec{r}) , \tag{14}$$

where V_{ext} is the external potential, V_H is the Hartree potential of the electronic charge density, and V_{xc} is the exchange-correlation (XC) potential, i.e., the functional derivative of the XC energy $E_{\text{xc}}[\rho]$:

$$V_{\text{xc}}[\rho](\vec{r})=\delta E_{\text{xc}}[\rho]/\delta\rho(\vec{r}) . \tag{15}$$

For the calculation of ground-state properties O (other than charge density or total energy) as a functional of the charge density the following formula applies:[16]

$$O[\rho]=O_0[\rho]+\Delta O[\rho] , \tag{16}$$

where $O_0[\rho]$ is the ground state (in exceptional cases, excited state[33]) expectation value with respect to a N-particle Slater determinant constructed from the self-consistent solutions of the Kohn-Sham equations and $\Delta O[\rho]$ is a correction functional which can be expressed as a derivative of the XC energy functional which belongs to a Hamiltonian containing the operator $\hat{o}$ via a scalar coupling constant λ (Ref. 16):

$$\Delta O[\rho]=(\partial/\partial\lambda)E_{\text{xc}}[\rho](\lambda)\,|_{\lambda=0} . \tag{17}$$

For the calculation of the momentum density the operator (in second quantization) $\hat{a}^{\dagger}_{\vec{p}}\hat{a}_{\vec{p}}$ has to be substituted for $\hat{o}$. Since ΔO is a derivative of the XC energy, it reflects the correction due to exchange and correlation effects which are not separable in a clear-cut way in density-functional theory. Still it makes sense to call ΔO a correlation correction in the case of the momentum density, since exchange effects are much smaller. In the homogeneous electron gas, for example, the neglect of exchange terms in the calculation of occupation numbers is inherent in the random-phase approximation, which gives good results, even for rather low densities.[32]

In actual calculations E_{xc} has to be approximated and errors are introduced, which will occur in the XC potential as well as for the correction term. Accurate experimental Compton profiles should be helpful in the process of analyzing if and where these approximations fail.

In Fig. 6 the final experimental result as listed in Table II is compared with the result of a band-structure calculation with a local density-functional potential for the valence electrons,[11] augmented by the atomic Compton profile of the argon configuration core of copper.[24] The linear combination of Gaussian orbitals method with a large basis set has been used in Ref. 11, which has the advantage that no shape approximations of the potential have to be introduced and that the (pseudo) wave functions are available in analytic form.[34] The achievement of a band-structure calculation of the Compton profile for the semiempirical Chodorow potential[35] can also be deduced from Fig. 6. It has been taken from Ref. 12 where the modified augmented plane-wave method has been employed. The same Hartree-Fock core Compton profiles[24] have been adopted here. The result of the Kohn-Sham equations in Fig. 6 is significantly different from that for the Chodorow potential, in contrast to the anisotropies, which are almost identical.[8] It is difficult to separate the effects of the different potentials from those which originate from the specific numerical methods, because the calculation of total Compton profiles is (just like the measurement) significantly more difficult than for the anisotropies.[8,34] The constant difference at higher momenta could, for example, be indicative for a not completely converged high-momentum integration limit in the calculation of the Compton profile from the momentum density in Eq.(1). Nevertheless, in the small momentum region the Chodorow potential seems to work somewhat better than the first-principles result, which agrees with the general experience.

On the other hand it is evident from Fig. 6 that the achievement of density-functional theory is improved

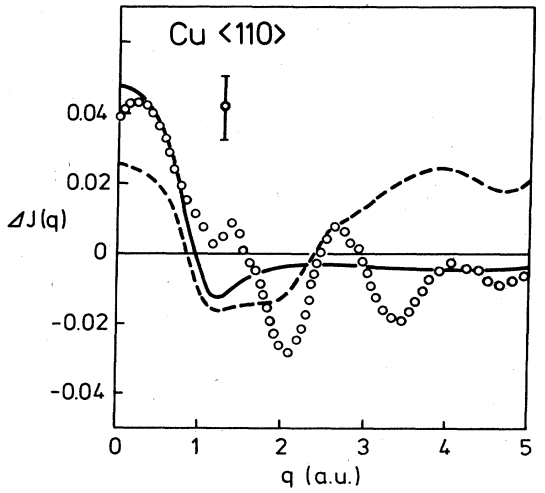

FIG. 6. Copper ⟨110⟩ Compton profiles. (a) Difference between the Kohn-Sham local density-functional band-structure theory (Ref. 11) augmented by Hartree-Fock free atomic core Compton profiles (Ref. 24) and the experiment (open circles). (b) Correction term obtained from $-\Delta n^{\text{LDA}}$ Eq. (18) (continuous curve). (c) Difference between the Kohn-Sham local density-functional theory (Ref. 11) and the Chodorow-potential band-structure theory (Ref. 12) (dashed curve). The theoretical results are convoluted by a Gaussian with a full width at half maximum of 0.41 a.u. of momentum to account for the experimental resolution smearing (Ref. 3).

beyond the Chodorow potential calculation, if the correlation correction functional (17) is considered. The correction term in the local density approximation (LDA):

$$\Delta n^{\mathrm{LDA}}[\rho]=\int \rho(\vec{r})\{n_0^h[\rho](\vec{r})-n_0^f[\rho](\vec{r})\}d\vec{r}\,, \quad (18)$$

where $n_0^h[\rho](\vec{r})-n_0^f[\rho](\vec{r})$ is the difference between the occupation numbers of the interacting and noninteracting homogeneous electron gas of density ρ, has been calculated from the occupation numbers of Ref. 32, which are sufficiently accurate for the present purposes.[8,36] The correction term takes into account the effect that in the homogeneous electron gas the Coulomb correlation excites electrons from occupied plane-wave states with wave vectors inside the Fermi surface into the unoccupied states outside the Fermi surface (see Fig. 5), which corresponds to a high-momentum tail in the Compton profiles. This effect is observed also for copper, since the agreement between theory and experiment is clearly improved by the incorporation of Δn^{LDA}. However, discrepancies remain in the form of a periodic modulation which per definition is a nonlocal correlation effect. This problem also occurs with respect to the results from the Chodorow potential.

At this point we would like to mention recent work on beryllium metal where thorough experimental[37,38] and theoretical[39–41] studies of the momentum density have been carried out. Of special interest in the present context are the local density-functional calculations of the Compton profiles of beryllium[40,41] which yield an almost perfect agreement with experiment for the anisotropies. As far as the total profiles are concerned, the agreement is significantly improved if the correlation correction (18) is considered[36,40–42] and the remaining discrepancies are very small. This result is consistent with the present work on copper, since nonlocal correlation effects are indeed expected to be much smaller for a simple metal such as beryllium with a relatively slowly varying charge density.

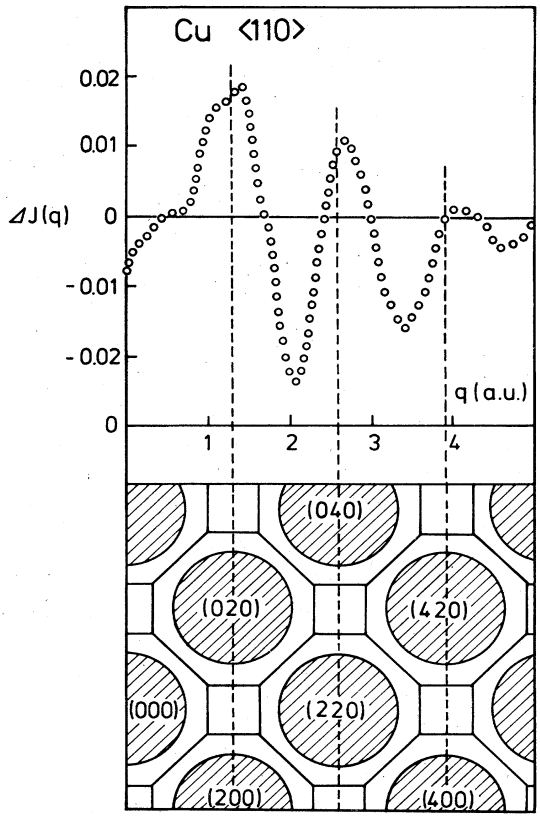

FIG. 7. Upper part: Difference between the local density-functional theory and the experiment (see text). Lower part: XY plane of the Brillouin zone and the Fermi surface of copper in the repeated zone scheme. The error bar of the experiment in Fig. 6 affects the general shape of the profile only. The oscillations shown here are much more significant.

C. Description of the correlation effect

In Fig. 7 the difference between local density-functional theory and experiment is displayed, where the correction term (18) has been included explicitly. The remaining discrepancy is essentially a periodic oscillation, which also corresponds to the difference observed between experimental and theoretical Compton profile anisotropies. The total correlation effect as far as resolved by the γ-ray Compton experiment consists then of an isotropic homogeneous-electron-gas-type contribution near the origin and an anisotropic $\cos(\vec{R}\cdot\vec{p})$ modulation of the Compton profiles with a wave vector $\vec{R}=(a/\sqrt{2})(\pm1,\pm1,0)$. It is the second term which is responsible for the significant renormalization mentioned in Sec. III A, which reduces the value of the Fourier transform of the Compton profile at the lattice vector. To trace the origin of the oscillations it is necessary to recall the reason for the existence of the Compton profile anisotropies, which might appear a bit surprising if one considers that the charge density can be described by the superposition of spherically symmetric (but not free atomic) charge densities centered on the nuclear positions. Originally this anisotropy has been explained by the Seitz wave-function model,[7] but the underlying principles become clearer by tight-binding model calculations.[9] The latter model proceeds from a minimal basis of atomic d orbitals and plane waves, taking into account the mixing between these states by empirically parametrized Hamiltonian matrix elements. Because of the hybridization between plane waves and d orbitals the unoccupied band states carry a small but significant d-electron character. Consequently, the occupied states with crystal momentum $\vec{k}$ outside the Fermi surface contain "d holes," which correspond to a discontinuously smaller momentum density for momenta which are equal to the wave vectors at the Fermi surface or differ by a reciprocal-lattice vector (see Fig. 8). By these discontinuities the hybridization projects images of the Fermi surface onto the momentum density, not only at the origin, but at all reciprocal-lattice vectors as indicated in Fig. 7. The Compton profiles (1) are derived from the momentum density by integration over planes normal to the scattering vector. The momentum density can in principle be completely reconstructed from a sufficiently large number of Compton profiles.[27] However, the finer details are lost in the experiment because of its resolution of 0.41 a.u. of momentum, which is almost one-third of the copper Fermi-surface diameter (1.44 a.u.). Only if the

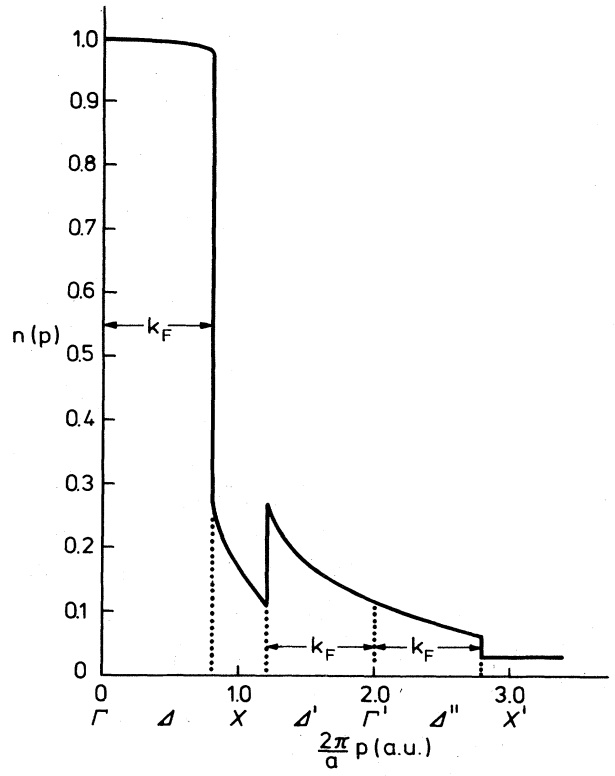

FIG. 8. Momentum density of copper in the ⟨110⟩ direction as obtained by the augmented plane-wave method for the Chodorow potential (Ref. 35). Capital letters indicate special points of the Brillouin zones and k_F denotes the length of the Fermi wave vector.

scattering vector is chosen normal to the planes relative to which all secondary Fermi surfaces are well aligned can one expect evidence of the hybridization effect. The lower part of Fig. 7 depicts a cross section of the reciprocal space and the intersections of some selected integration planes normal to the ⟨110⟩ direction. By some consideration of the three-dimensional structure of the reciprocal lattice for the fcc unit cell, one can be convinced that this direction is the only one which fulfills the above requirements. It has indeed been found that the Compton profile anisotropies are clearly larger if the ⟨110⟩ direction is involved, which show extrema when the integration plane cut through reciprocal-lattice vectors, i.e., at $p=n(2\pi\sqrt{2}/a)$ a.u., or just in between, i.e., at $p=(n+1/2)(2\pi\sqrt{2}/a)$ a.u., where n is an integer. Despite this the charge density is allowed to be essentially spherically symmetric because the Fermi surface is, so that hybridization involves the e_g and t_{2g} atomic states to the same extent. This situation is somewhat different in vanadium, where the charge density shows significant deviations from spherical symmetry (see, e.g., Ref. 43 and references therein). In the Compton profiles[44] this "wave-function anisotropy" is reflected by a slowly varying modulation superimposed onto the more rapidly varying "occupation anisotropy" which was found in copper.

For an explanation of the effect one first has to exclude the possibility that the observed discrepancies in Fig. 7 are a consequence of an improper description of the hybridization effect in the band-structure equations. This has been achieved by showing that a reduction of the hybridization, which would improve the agreement for the Compton profile anisotropies, is prohibited by the corresponding deterioration of the results for the charge density, which is the quantity where the Kohn-Sham equations in principle aim at.[8] The band structure and Fermi surface resulted in being changed for the worse also. Since the discrepancies between experimental and theoretical anisotropies are identified to originate from the ⟨110⟩ directional Compton profile, the above argument can be carried over to the total profile.

The correlation effect in the *homogeneous* electron gas (see Fig. 5) corresponds to a transfer of momentum density from the occupied Fermi surface into the unoccupied region as discussed above. The upper curve in Fig. 7 provides then for a strong indication that in the *inhomogeneous* electron gas the same effect is observable not only for the primary Fermi surface, but also for its images centered at reciprocal-lattice vectors, i.e., a transfer of momentum density into the interstitial regions where the momentum density is small, thus washing out the contrast predicted by the one-electron model. In principle a similar effect is expected also for simple metals,[45,46] but as mentioned above, it could not be observed for beryllium.[42]

IV. DISCUSSION

In this section we want to investigate if and how the observations can be explained or calculated by the means available today for the description of the properties of the inhomogeneous electron gas. By elimination of unsuitable approaches some conclusions can be drawn, although the discussion must remain qualitative.

A. Nonlocal correlations in density-functional theory

We shall start this section by a discussion of the role of nonlocal correlation effects in the density-functional theory of Hohenberg, Kohn, and Sham and how the observations described above fit in the present understanding of the subject.

A revealing contribution to density-functional theory is the adiabatic connection approach[33] according to which the XC energy functional may be written as

$$E_{\rm xc}[\rho]=\int d\vec{r}\rho(\vec{r})\int d\vec{r}'\rho_{\rm xc}[\rho](\vec{r},\vec{r}')/|\vec{r}-\vec{r}'|\ , \tag{19}$$

where

$$\rho_{\rm xc}[\rho](\vec{r},\vec{r}')=\int_0^1 dg\rho_{\rm xc}[\vec{\rho}](\vec{r},\vec{r}';g)\ . \tag{20}$$

$\rho_{\rm xc}(g)$ is the XC hole of an electron in a hypothetical system where the electron-electron interaction coupling constant g may vary between 0 and the physical value of 1, and where the charge density is kept constant for all g by an additional effective one-particle potential. It follows from (14) that it is not necessary to know the XC hole in complete detail for a calculation of the energy.[47] Only the

spherical average, i.e., the average over angular coordinates $\hat{r}'$,

$$\rho_{xc}(\vec{r},|\vec{r}'|)=(1/4\pi)\int d\hat{r}'\rho_{xc}(\vec{r},\vec{r}')\,, \tag{21}$$

contributes to the integral over $\vec{r}'$ in (19).[47] The local density approximation corresponds to replacing ρ_{xc} by the isotropic XC hole of the homogeneous electron gas. By model calculations it has been shown that in strongly inhomogeneous systems ρ_{xc}^{h} is different from the real XC hole, but since only the spherical average is of importance, the errors cancel to a large extent in the calculation of the energy and the result is still quite satisfactory. The XC hole is not an observable but it will be shown now that by a transformation into momentum space the argument is directly supported by the experimental result presented here. At zero pressure the virial theorem reads

$$E[\rho]=-T[\rho]\,. \tag{22}$$

The kinetic energy T can be expressed in terms of the momentum density and Compton profiles:

$$T[\rho]=\int d\vec{p}\,p^2 n[\rho](\vec{p})=\int dq\,q^2 J_h[\rho](q)\,, \tag{23}$$

where $\vec{h}$ is arbitrary here. It has been proven recently[48] that the virial theorem also holds for the locally approximated functionals:

$$E^{\mathrm{LDA}}[\rho^{\mathrm{LDA}}]=-T^{\mathrm{LDA}}[\rho^{\mathrm{LDA}}]\,. \tag{24}$$

Neglecting the small difference between ρ and ρ^{LDA},

$$E-E^{\mathrm{LDA}}=E_{xc}^{\mathrm{NL}}=-T_{xc}^{\mathrm{NL}}\,, \tag{25}$$

$$E_{xc}^{\mathrm{NC}}=\int dq\,q^2[J_{\vec{h}}^{\mathrm{LDA}}(q)-J_{\vec{h}}^{\mathrm{expt}}(q)]\,. \tag{26}$$

The term in square brackets in the integral of (26) is plotted in Fig. 7. The measured profile is unfortunately not accurate enough to provide for a reliable estimate of the nonlocal kinetic energy. However, the striking oscillations in the $\langle 110\rangle$ profile, which reflect the anisotropic correlation effect, cancel in the integration and do not contribute to the energy. Thus despite significant anisotropic nonlocal effects we can expect that the local density approximation provides for an appropriate representation of the total energy functional and eventually also for the charge density, which is obtained by minimizing this functional. Vice versa, the rather small errors in the energy functional are amplified in its derivative. This finding can be compared with the results of Ref. 49, where in spite of a reasonable accuracy of E_{xc}^{LDA} for small atoms, the XC potential $\delta E_{xc}/\delta\rho$ resulted to be less satisfactorily reproduced by the LDA.

Several proposals exist of how nonlocal effects can be incorporated to improve upon the local density approximation. As examples we mention here the self-interaction correction in different implementations,[50–52] the weighted and/or average density approach[53] and an effective gradient expansion.[54] All these approaches essentially lean on an isotropic behavior of the electron correlation and attempt an improvement of the spherical average of the XC hole only. In the present form all these proposals do not seem to provide a satisfactory description of the anisotropic correlation effects which cancel in the energy calculation. In Ref. 55 it has been argued that the anisotropies in the electron correlation are quenched by the gradient expansion from which the interpretation as a many-body quantum interference term derives.

B. Relation to spectral properties

The electronic momentum density is intimately related to the spectral properties of the system via the diagonal elements of the spectral density function A in the momentum representation by Eq. (6). $A(\omega)$ can be measured by photoemission experiments[4] as a function of energy. If the samples are single crystals and the photoelectrons are detected as a function of emission angle, it is possible to determine the $\vec{k}$-space dispersion of the peaks in the spectrum, which is the quasiparticle band structure. Recently there has been a lot of interest in the appearance of satellite structures to the main signals which usually occur at higher binding energies and which cannot be explained by a one-electron picture.[56] We believe that our experiments have to be explained also by satellite structures. The absence of any limiting Fermi vector allows for an increased momentum density in the interstitial regions in Fig. 7, while also a reduction of the spectral strength from the quasiparticle close to the Fermi surface will be implied.

In nickel a valence-band satellite is clearly observed and explained by predominantly atomiclike correlations of the d electrons.[56] In the homogeneous electron gas, resonance structures are expected as a direct consequence of the plasmon singularity in the dielectric function.[57] These excitations have been called plasmarons, which stresses its origin from a collective effect. In silver, collective excitations are revealed by uv reflectance spectra.[58] Copper is more or less intermediate between nickel and silver. In copper the d bands are closer to the Fermi energy than in silver with the result that the plasmons decay very quickly due to interband transitions.[58] On the other hand, the d bands are too far from the Fermi energy to allow for an appreciable atomic correlation effect as in nickel. This conclusion can be drawn from photoemission experiments,[59] where only a very weak atomic multiplet structure is observed, which can be hardly responsible for our observations. The elusiveness of the supposed resonances for photoemission experiments does not mean that they do not exist, but only that they do not appear as well-defined peaks, but as broader structures, which is equivalent to a short lifetime. It is thus perhaps better to speak about dissipative processes instead of resonances or satellites. The broadness of the features, however, is of no concern for the results of Compton-scattering experiments as long as the energy integral is large enough. This is a distinct advantage of this technique which makes it truly complementary to photoemission, where, on the other hand, signals can be resolved which do not have to contribute much to the integral as long as they are sufficiently peaked.

A first computational approach could be the solution of the quasiparticle equations with a local approximation to the electronic self-energy,[60] explicitly taking into account the plasmaron pole.[57] Qualitatively, the agreement with

the experiment is expected to improve, although for quantitative agreement a more sophisticated approach is needed, because as outlined in Sec. III A, the observed effect is larger than in the homogeneous electron gas, by which a locally approximated self-energy would have to be parametrized.

C. Momentum density-functional theory

As an alternative to the Hohenberg-Kohn-Sham charge density-functional theory there exists an energy functional of the momentum density,[61] which is minimal and equal to the ground-state energy for the ground-state momentum density. If analogously to the derivation of the Kohn-Sham equations a set of self-consistent single-particle equations could be found by minimization of this functional, an algorithm would be available for the calculation of Compton profiles without the *a posteriori* correction term which causes the difficulties here. Unfortunately this program cannot be carried out for a fundamental reason. To show this we recall that the Kohn-Sham equation relies on the (unproven) assumption of the so-called noninteracting wave function V representability,[62] which means that the charge density of the many-body ground state must be representable by a one-determinant wave function, where the orbitals are eigenfunctions of a single-particle Hamiltonian with an effective potential which is local in the sense that it is a multiplicative operator in position space. The corresponding set of one-particle equations in momentum space can be derived if a noninteracting wave function "T representability"[63] is assumed, which means that the many-body ground-state momentum density can be represented by the wave functions coming from a single-particle Hamiltonian with an effective kinetic energy operator which has to be local in momentum space. The solutions of these single-particle equations must be Bloch waves, and the corresponding momentum density is topologically identical to that derived from the Kohn-Sham equations. But the occupation number effect discussed above cannot be represented by a single determinant of Bloch waves. This T representability thus breaks down for the description of the momentum density, and we have to reject this idea for our present purposes.[63]

V. CONCLUSIONS

Compton-scattering experiments on copper single crystals have revealed an electron correlation effect which is clearly enhanced compared to simple metals. It can be described qualitatively, but cannot be calculated quantitatively by the methods which are usually applied for a first-principles treatment of the inhomogeneous electron gas. We hope that our experiment will motivate new theoretical efforts directed at an improved description of the ground-state properties and the one-particle valence-band excitation spectrum of copper.

*Present address: The Institute for Solid State Physics, The University of Tokyo, Roppongi, Minato-ku, Tokyo, 106 Japan.

[1]P. M. Platzman, Comments Solid State Phys. B **4**, 85 (1972).
[2]P. M. Platzman and N. Tzoar, in *Compton Scattering,* edited by B. G. Williams (McGraw-Hill, New York, 1977).
[3]P. Pattison and J. R. Schneider, Nucl. Instrum. Methods **159**, 145 (1979).
[4]N. V. Smith and F. J. Himpsel, in *Handbook of Synchrotron Radiation,* edited by E. E. Koch (North-Holland, Amsterdam, 1983), Vol. 1B.
[5]J. R. Schneider, Nucl. Sci. Appl. **1**, 227 (1981).
[6]J. R. Schneider, Fortschr. Mineral. **61**, 1 (1983).
[7]P. Pattison, N. K. Hansen, and J. R. Schneider, Z. Phys. B **46**, 285 (1982).
[8]G. E. W. Bauer and J. R. Schneider, Z. Phys. B **54**, 17 (1983).
[9]G. E. W. Bauer and J. R. Schneider, J. Phys. Chem. Phys. **45**, 675 (1984).
[10]G. E. W. Bauer and J. R. Schneider, Phys. Rev. Lett. **52**, 2061 (1984).
[11]D. Bagayoko, D. G. Laurent, S. P. Singhal, and J. Callaway, Phys. Lett. **76A**, 187 (1980).
[12]H. Bross, J. Phys. F **12**, 2249 (1982).
[13]P. Hohenberg and W. Kohn, Phys. Rev. **136**, B864 (1964).
[14]W. Kohn and L. J. Sham, Phys. Rev. **140**, A1133 (1965).
[15]L. Lam and P. M. Platzman, Phys. Rev. B **9**, 5122 (1974).
[16]G. E. W. Bauer, Phys. Rev. B **27**, 5912 (1983).
[17]P. Eisenberger and W. A. Reed, Phys. Rev. B **8**, 3242 (1974).
[18]V. Halonen, I. R. Epstein, A. C. Tanner, and B. G. Williams, in *Compton Scattering,* edited by B. G. Williams (McGraw-Hill, New York, 1977).
[19]G. E. W. Bauer and P. Pattison, Hahn-Meitner-Institute (HMI) Internal Report No. B364, 1981 (unpublished).
[20]W. Weyrich, Ber. Bunsenges. Phys. Chem. **79**, 1085 (1975).
[21]J. Felsteiner and P. Pattison, Nucl. Instrum. Methods **124**, 449 (1980).
[22]S. Krinsky, M. L. Perlmann, and R. E. Watson, in *Handbook of Synchrotron Radiation,* edited by E.-E. Koch (North-Holland, Amsterdam, 1983), Vol. 1A.
[23]J. Felsteiner and P. Pattison, Phys. Rev. B **13**, 1702 (1976).
[24]F. Biggs, L. B. Mendelssohn, and J. B. Mann, At. Data Nucl. Data Tables **16**, 201 (1975).
[25]G. E. W. Bauer, J. Felsteiner, and J. R.Schneider, Hahn-Meitner-Institute (HMI) Internal Report No. B 412, 1984 (unpublished), p. 155.
[26]G. E. W. Bauer, Ph.D. thesis, Technische Universität Berlin, 1984 (unpublished).
[27]P. E. Mijnarends, in *Positron Solid State Physics, Proceedings of the International School of Physics Enrico Fermi,* edited by W. Brandt and A. Dupasquier (North-Holland, Amsterdam, 1983).
[28]S. Berko, in *Positron Solid State Physics, Proceedings of the International School of Physics Enrico Fermi,* edited by W. Brandt and A. Dupasquier (North-Holland, Amsterdam, 1983).
[29]D. G. Lock, V. H. C. Crisp, and R. N. West, J. Phys. F **3**, 561 (1973).
[30]L. Hedin and S. Lundqvist, in *Solid State Physics,* edited by F. Seitz and D. Turnbull (Academic, New York, 1969), Vol. 23, p. 1.
[31]W. Schülke, Phys. Status Solidi B **82**, 229 (1977).
[32]B. I. Lundqvist, Phys. Kondens. Mater. **7**, 117 (1968).
[33]J. Harris, Phys. Rev. A **29**, 1648 (1984).
[34]A. K. Ray and S. B. Trickey, Phys. Rev. B **24**, 1751 (1981).

[35]M. I. Chodorow, Ph.D. thesis, Massachusetts Institute of Technology, 1939 (unpublished).
[36]G. E. W. Bauer and J. R. Schneider, Solid State Commun. **47**, 673 (1983).
[37]N. K. Hansen, P. Pattison, and J. R. Schneider, Z. Phys. B **25**, 215 (1979).
[38]G. Loupias, J. Petiau, A. Isolah, and M. Schneider, Phys. Status Solidi B **102**, 79 (1980).
[39]R. Dovesi, C. Pisani, F. Ricca, and C. Roetti, Z. Phys. B **47**, 19 (1982).
[40]M. Y. Chou, P. K. Lam, M. L. Cohen, G. Loupias, J. Chomillier, and J. Petiau, Phys. Rev. Lett. **49**, 1452 (1982).
[41]M. Y. Chou, P. K. Lam, and M. L. Cohen, Phys. Rev. B **28**, 1696 (1983).
[42]P. Rennert, Phys. Status Solidi B **105**, 567 (1981).
[43]H. R. Kretschmer and J. R. Schneider, Solid State Commun. **49**, 971 (1983); Naturwissenschaffen (to be published).
[44]A. J. Rollason, R. S. Holt, and M. J. Cooper, Philos. Mag. B **47**, 51 (1983).
[45]B. I. Lundqvist and C. Lydén, Phys. Rev. B **4**, 3360 (1971).
[46]P. Eisenberger, L. Lam, P. M. Platzman, and P. Schmidt, Phys. Rev. B **6**, 3671 (1972).
[47]O. Gunnarson and B. I. Lundqvist, Phys. Rev. B **13**, 4274 (1976).
[48]U. von Barth and A. R. Williams, in *Theory of the Inhomogeneous Electron Gas,* edited by N. H. March and S. Lundqvist (Plenum, New York, 1983).
[49]C.-O. Almbladh and A. C. Pedroza, Phys. Rev. A **29**, 2322 (1984).
[50]J. P. Perdew and A. Zunger, Phys. Rev. B **23**, 5048 (1981).
[51]J. P. Perdew and M. Norman, Phys. Rev. B **26**, 5448 (1982).
[52]R. A. Heaton, J. G. Harrison, and C. C. Lin, Phys. Rev. B **28**, 5992 (1983).
[53]O. Gunnarson, M. Jonson, and B. I. Lundqvist, Phys. Rev. B **20**, 3176 (1979).
[54]D. C. Langreth and M. J. Mehl, Phys. Rev. B **28**, 1809 (1983).
[55]G. E. W. Bauer, Phys. Rev. B **30**, 1010 (1984).
[56]C.-O. Almbladh and L. Hedin, in *Handbook of Sychrotron Radiation,* edited by E. E. Koch (North-Holland, Amsterdam, 1983), Vol. 1B.
[57]B. I. Lundqvist, Phys. Kondens. Mater. **6**, 206 (1967).
[58]H. Ehrenreich and H. R. Phillip, Phys. Rev. **128**, 1622 (1962).
[59]H. Iwan, F. J. Himpsel, and D. E. Eastman, Phys. Rev. Lett. **43**, 1829 (1979).
[60]L. J. Sham and W. Kohn, Phys. Rev. **145**, 561 (1966).
[61]G. A. Henderson, Phys. Rev. A **23**, 19 (1981).
[62]M. Levy, Phys. Rev. A **26**, 1200 (1982).
[63]G. E. W. Bauer (unpublished).